frontiers | Frontiers in Astronomy and Space Sciences

TYPE Original Research
PUBLISHED 24 April 2024
DOI 10.3389/fspas.2024.1368633

OPEN ACCESS

EDITED BY
Alberto Rodriguez-Ardila,
Laboratório Nacional de Astrofísica, Brazil

REVIEWED BY
Zhiyuan Ma,
University of Massachusetts Amherst, United States
Filiberto Hueyotl-Zahuantitla,
Cátedra CONACYT-UNACH, Mexico

*CORRESPONDENCE
Lev Titarchuk,
titarchuk@fe.infn.it

RECEIVED 10 January 2024
ACCEPTED 13 March 2024
PUBLISHED 24 April 2024

CITATION
Titarchuk L and Seifina E (2024), SDSS J075217.84 + 193542.2: X-ray weighing of a secondary BH.
Front. Astron. Space Sci. 11:1368633.
doi: 10.3389/fspas.2024.1368633

SDSS J075217.84 + 193542.2: X-ray weighing of a secondary BH

Lev Titarchuk[1]* and Elena Seifina[2]

[1]Dipartimento di Fisica, University di Ferrara, Ferrara, Italy, [2]Lomonosov Moscow State University, Sternberg Astronomical Institute, Universitetsky Prospect 13, Moscow, Russia

Precise measurements of black hole (BH) masses are necessary to understand the coevolution of these sources and their host galaxies. Sometimes in the center of a galaxy, there is not one but two BHs. The BH duality of the quasar nucleus SDSS J075217.84 + 193542.2 (herein referred to as SDSS J0752) was recently proposed based on the observed strict periodicity of optical emission from the source. We tested this assumption using X-ray observations obtained using Swift/XRT (2008–2010). We fitted the SDSS J075217 spectrum using a Comptonization model and discovered soft X-ray variability in the 0.3–10-keV energy range. We pursued a scenario in which two supermassive BHs at the center of SDSS J0752 form a pair, and the less massive (secondary) BH periodically crosses/punctures the disk around the more massive (primary) BH. We associated these periodic crossings with tidal disruptions of the disk and, as a consequence, with an increase in X-rays observed as a flare in SDSS J0752. During such an X-ray flare event (2008–2010), we discovered a change in the source spectral states and the photon index saturation at the $\Gamma \sim 3$ level with mass accretion rate $\dot{M}$. For BH mass scaling, we used OJ 287, M101 ULX–1, and HLX–1 ESO 243–49 as reference sources and found that $M_{SDSS} = 9 \times 10^7$ solar masses, assuming that $d_{SDSS} = 500$ Mpc. Thus, we obtained a lower limit to a BH mass due to the unknown inclination. In addition, we used the virial mass of the secondary BH based on H_α-line measurements, and we estimated the inclination of the binary at SDSS J0752, $i = 80°$, using a scaling technique.

KEYWORDS

accretion, accretion disks, black hole physics, galaxies: active galaxies, individual SDSS J075217.84 + 193542.2

1 Introduction

The duality of objects is a fairly common phenomenon in astrophysics. Most stars in the universe are binary. Duality is also common among galaxies. Over the past few years, the number of detected binary black holes (BHs) in the centers of galaxies has increased sharply. Although such double objects are no longer uncommon, the manifestation of their binarity remains not fully understood. Analysis of the dual nature of BHs in active galactic nuclei (AGNs) confirms the reality of supermassive BH (SMBH) mergers in galactic nuclei. Scientists have long been concerned about the problem of the origin of ultra-massive BHs, because due to matter accretion onto stellar-mass BHs, they could not form since this would require time longer than the lifetime of the universe. The discovery of binary AGNs, observations of massive BH merger events, and confirmations of the high resulting masses of such BHs obtained in recent years are a real breakthrough in our understanding of the origin of ultra-massive BHs through massive BH mergers in galactic nuclei.

Binary supermassive BHs are a remarkable by-product of galaxy mergers in the hierarchical universe (Begelman et al., 1980). In the very last stage of their orbital evolution, gravitational wave radiation powers the binary inspiral. Periodic X-ray/optical/radio flares from AGNs during their orbital rotation have been proposed as a powerful tool for studying such binary systems (Liu et al., 2016; Chen et al., 2020). It should be noted that the very idea of binary systems with SMBHs was expressed by Komberg (1967). Subsequently, their hypothesis about the possible duality of nuclei in quasars was brilliantly confirmed by observations (Section 3). However, the methods for establishing the duality of SMBHs are tenuous at best and are based on four criteria (Seifina, 2024).

First, the duality of galactic nuclei is, in some cases, demonstrated by analyzing their observed images (for nearby galaxies), which allows us to resolve the double structure of their central regions (for example, NGC 7727; Voggel et al. (2022); NGC 6240; Kollatschny et al. (2020); Mrk 739; Koss et al. (2011); and UGC 4211; Koss et al. (2023)). For distant AGNs, spectroscopic studies make it possible to establish duality by the characteristic behavior of spectral line systems [SDSS J1537 + 044; Boroson and Lauer (2009); SDSS J0927 + 294; Eracleous et al. (2012)]. It is clear that the described methods are no longer applicable for very distant sources. In fact, the collision of galaxies (and, accordingly, their nuclei) in the past led to the formation of a binary system from two SMBHs; however, there is no definitive way to indicate the duality of their new "nucleus," except perhaps for the presence of "extra" jets in 3C 75 (Molnar et al., 2017) or the strict periodicity of the source flares in OJ 287 (Zhang, 2022; Titarchuk et al., 2023). In such cases, the duality of the nucleus can sometimes be established by individual exotic features, for example, by the same bending of the jets of each of the SMBHs, by the specific shape of the light curve (for example, from periodicity and from the double-humped flare maximum in the light curve), or as a possible way to connect the results on optical, X-ray, and radio data for the same object. As an interesting additional criterion for duality, Titarchuk et al. (2023) pointed to the duality of SMBHs in an AGN, established by peculiarities, i.e., the discrepancy between the BH mass according to X-ray and optical data as a possible consequence of the duality of the central AGN in M87 [Titarchuk et al. (2023; 2020); Seifina (2024)].

Binary BHs in distant quasars are of particular interest and complexity. Because of their remoteness, it is impossible to establish the duality of their nuclei by direct imaging or Doppler shift analysis of spectral lines. Therefore, the main method for establishing their duality is through analysis of the periodicity of radiation from such sources, which may reveal quasi-periodic oscillations (QPOs) of their emission.

Recently, a QPO with a periodicity of 6.4 years was discovered in the SDSS J075217.84 + 193542.2 quasar (herein referred to as SDSS J0752) by Zhang (2022) at a redshift of 0.117 (Paris et al., 2018). The discovery of this QPO made this quasar a reliable candidate for the binary systems containing SMBHs. In fact, the BH duality in the SDSS J0752 center is indicated by the detection of two Gaussian components in the broad H_α line, with an expected spatial distance of approximately 0.02 pc between these two central SMBHs.

TABLE 1 Basic parameters of SDSS J0752.

Parameter	Value	Reference
Source class	QSO	Zhang (2022)
Virial mass of a primary black hole (BH), $M_\odot$	$\sim 1.04 \times 10^9$	Zhang (2022)
Virial mass of a secondary BH, $M_\odot$	$\sim 8.8 \times 10^7$	Zhang (2022)
Orbital inclination, *i*, deg	~ 80	This work
Orbital period, P, yr	6.4	Zhang (2022)
Distance *D*, Mpc	~ 500	This work
Redshift, *z*	0.117	Paris et al. (2018)

Their virial masses are approximately $8.8 \times 10^7 M_\odot$ and $1.04 \times 10^9 M_\odot$ (Table 1).

This periodicity is derived from the analysis of the 13.6-year optical light curve from the Catalina Sky Survey (CSS) (Drake et al., 2009) and from the All Sky Automated Survey for SuperNovae (ASAS-SN) (Shappee et al., 2014; Kochanek et al., 2017). The 6.4-year QPOs are also confirmed using the generalized Lomb–Scargle periodogram with a confidence level of above 99.99%, as well as using the results of autocorrelation analysis and using the weighted wavelet z-transformation technique.

In this paper, we test the binary BH hypothesis in SDSS J0752 (schematically presented in Figure 1) using Swift/XRT data obtained from an X-ray counterpart of this source (Figure 2). The specific goal of our paper is to estimate the mass of the secondary BH in SDSS J0752 applying the scaling method to determine the mass of the BH (Shaposhnikov and Titarchuk (2009), hereafter referred to as ST09) based on *Swift* observations obtained during X-ray flaring events (Figure 3). Based on the discovered more or less strict 6.4-year cycle, we adhere to the hypothesis of the orbital rotation of components in a binary BH, in which the secondary BH periodically disturbs the accretion disk around the primary BH (Figure 1) to explain the optical (and possibly X-ray) periodic variability of SDSS J0752 (Zhang, 2022). In this case, the secondary BH is surrounded by a smaller disk, a minidisk, consisting of matter captured during such periodic passages of the primary BH disk (Figure 1).

The scaling method was proposed by Shaposhnikov and Titarchuk (2007), hereafter referred to as ST07, and by ST09. It is worth noting that there are two scaling methods: based on the correlation between the photon index, Γ, and the QPO frequency, ν_L, and based on the correlation between Γ and the normalization of the spectrum proportional to $\dot{M}$. For the first method ($\Gamma - \nu_L$), the source distance is not required to estimate the BH mass (ST07), while for the second method, $\Gamma - \dot{M}$ (see ST09), the source distance and the inclination of the accretion disk relative to the Earth observer are needed.

For both methods, it is necessary for the source to show a change in spectral states, accompanied by a characteristic behavior of the index Γ during the flare. Γ monotonically increases with ν_L or $\dot{M}$

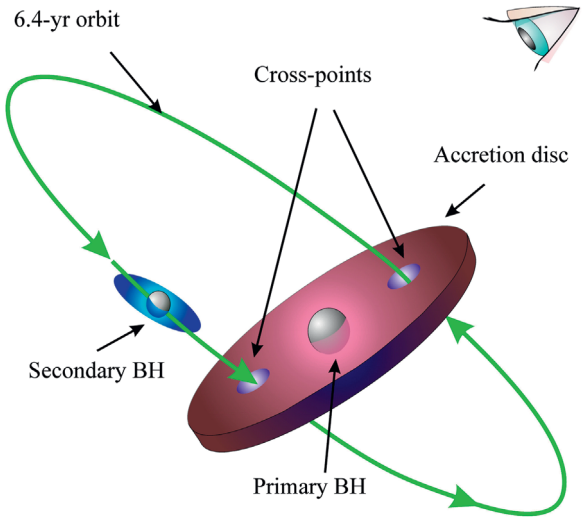

FIGURE 1
Schematic diagram of the SDSS J0752 model used in our analysis.

during the transition from the low-hard state (LHS) through the intermediate state (IS) to the high–soft state (HSS) and reaching a constant level (saturating) at high values of ν_L or $\dot{M}$. Then, Γ monotonically decreases during an HSS → IS → LHS transition when the flare decays. The saturation of Γ (the so-called Γ-saturation phase whereby Γ reaches a constant value in our parameter space; see Figure 6) during a flare is a specific indication that this particular object contains a BH (Titarchuk and Zannias, 1998). Indeed, the Γ-saturation phase can be only caused by an accretion flow converging to the event horizon of a BH [see numerical simulation results obtained by Laurent and Titarchuk (1999); Laurent and Titarchuk (2011)]. Then, it makes sense to compare BH sources that have the same Γ-saturation levels. In the second method ($\Gamma - \dot{M}$), it is assumed that BH luminosity is directly proportional to $\dot{M}$ (and, consequently, to the mass of the central BH) and inversely proportional to the squared distance to the source. Thus, we can determine the BH mass by comparing the corresponding tracks $\Gamma - \dot{M}$ for a pair of sources with BHs, in which all parameters are known except for the BH mass (more details on the scaling method are given in the studies by Titarchuk et al. (2010); Seifina and Titarchuk (2010); and ST09).

The scaling approach, in general, has a number of advantages over other methods for the determination of a BH mass. A determination of the X-ray spectrum arising from the innermost part of the source, based on fundamental physical models, takes into account the Comptonization of soft disk photons by hot electrons from the Compton cloud and in the converging flow into a BH. In this case, the latest achievements in modeling the BH states using the Monte Carlo method were used based on the numerical solution of the complete relativistic kinetic equation and the detection of the "saturation" phase of the spectral index at the maximum of the X-ray flare of the BH. We developed and tested the method on various astrophysical objects, and the results showed excellent agreement with classical methods (see, e.g., Seifina and Titarchuk (2010); Titarchuk et al. (2014); Titarchuk and Seifina (2016a), Titarchuk and Seifina (2017); Seifina et al. (2017); Seifina et al. (2018b); Titarchuk et al. (2020); Titarchuk and Seifina (2023). The method is based on the first principles and fundamental assessments of the gravitational effect of a BH on the matter surrounding it, as well as on calculating the effective size and mass of the reaction zone to such an effect.

In this paper, based on a particular *Swift/XRT* data analysis, we estimate a BH mass in SDSS J0752 using the scaling method. Section 2 provides the details of our data analysis; Section 3 presents a description of the spectral models used for fitting these data and results; Section 4 discusses the main results of the paper. In Section 5 we present the conclusion.

2 Data reduction

Using *Swift*/XRT data in the 0.3–10-keV energy range, we studied flaring events of SDSS J0752 from 2008 to 2010 (see the log of observations in Table 2). The data used in this paper are publicly available through the GSFC public archive[1]. It must be noted that not all flare events can be associated with the disk–secondary BH interactions. Therefore, it is difficult to separate the sporadic flares that often occur in SDSS J0752, which are completely unrelated to the presence of any binary system in the SDSS J0752 center**.** However, the identified periodicity of the optical source facilitates such identification since it can be associated mainly with orbital variability. Here, we assume that X-ray variability is caused by flares due to the passage of a smaller BH through the disk around a larger BH. Moreover, it will be accompanied by corresponding spectral changes, which will help us separate the X-ray flare activity of the small BH. Section 3 presents the X-ray variability analysis of SDSS J0752 (using Swift/XRT) and shows that SDSS J0752 follows spectral patterns typical of galactic and extragalactic sources with BHs.

Data were processed using HEASoft v6.14, the `xrtpipeline` tool v0.12.84, and the calibration files (CALDB version 4.1). The ancillary response files were created using `xrtmkarf` v0.6.0, and exposure maps were generated using `xrtexpomap` v0.2.7. Source events were accumulated within a circular region with a radius of 50″ centered at the position of SDSS J0752 ($\alpha = 07^h52^m17^s.63$ and $\delta = +19°35'42''.7$, J2000.0). Given the low count rate of SDSS J0752, most of the data were collected using the most sensitive photon counting (PC) mode. The background was estimated in a nearby source-free circular region with a radius of 85″.

Using the `xselect` v2.4 task, source and background light curves and spectra were generated. Spectra were rebinned with at least 10 counts in each energy bin using the `grppha` task in order to apply χ^2 statistics. We also used the online XRT data product generator[2] to obtain the image of the source field of view (FOV) in order to make a visual inspection and remove possible contamination from nearby sources (Evans et al., 2007;

1 https://heasarc.gsfc.nasa.gov

2 http://www.swift.ac.uk/user_objects/

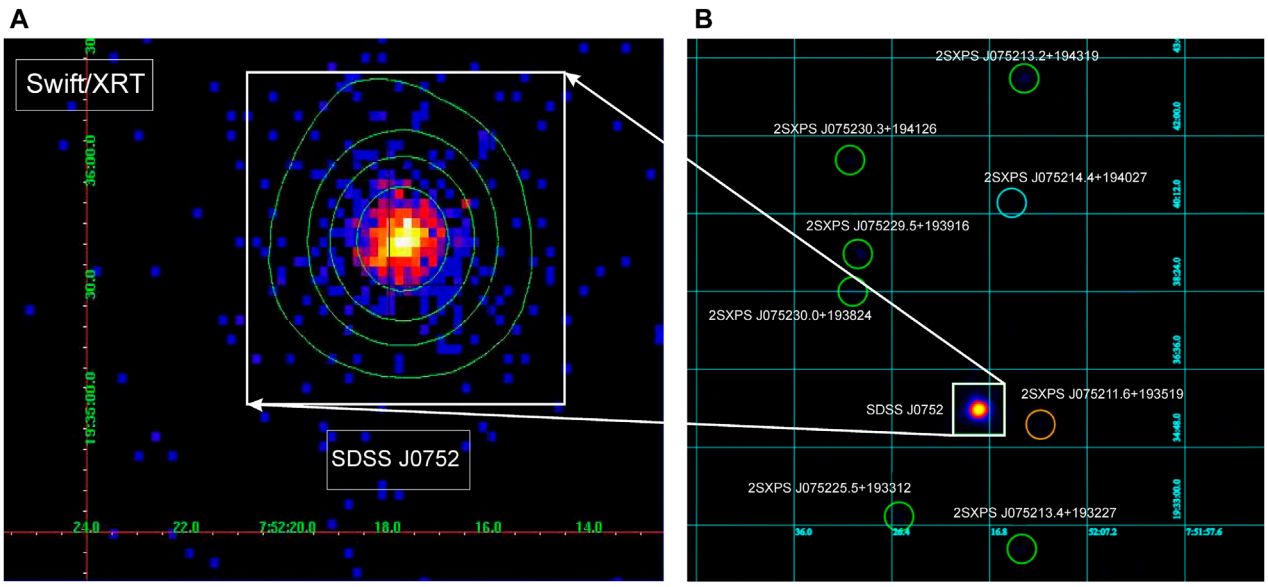

FIGURE 2
Swift X-ray image of SDSS J0752, accumulated from 31 October 2008 to 30 May 2010 with an exposure time of 14 ks. Green contours in an enlarged image **(A)** of SDSS J0752 confirm the absence of other nearby objects in the 1.3′ field of view (FOV); this image is 160 pixels (=6.3′ to a side). SDSS J075217.7 + 193540 is indicated by the white box in the panel **(B)**, while the rest of the sources of the FOV are marked with circles and corresponding names from the 2SXPS catalog. The next nearest source (indicated by the orange circle) is 86″ away.

TABLE 2 List of the *Swift* observations of SDSS J0752 used in our analysis.

Obs. ID	Start time (UT)	Exposure time (ks)	Start time (MJD)
00038041001	2008 October 31, 07:06:59	3.6	54,770.297
00038041002	2009 February 24, 04:55:17	1.3	54,886.205
00038041003	2009 September 12, 19:12:59	1.5	55,086.800
00038041004	2010 May 30, 00:07:16	2.7	55,346.005
00039551001	2010 May 30, 09:44:39	5.0	55,346.406

Evans et al., 2009). The *Swift*/XRT (0.3–10 keV) image of the SDSS J0752 FOV is given in the right panel of Figure 2, where panel (a) demonstrates the absence of the X-ray jet-like (elongated) structure and the minimal contamination by other point sources and diffuse emission within a region with a radius of 85″ around SDSS J0752. The next nearest source 2SXPS J075211.6 + 193519 is 86″ away (marked by the orange circle). We used the *Swift* observation of SDSS J0752 (2008–2010) extracted from the HEASARC and found that these data cover a wide range of X-ray luminosities.

Before proceeding and providing the details of the spectral fitting, we study the long-term behavior of SDSS J0752, in particular, its activity patterns. We present a long-term X-ray light curve of SDSS J0752 detected using the XRT on board *Swift* from 2008 to 2010 (see Figure 3).

We note that this X-ray light curve makes it rather difficult to judge the 6.4-year periodicity found earlier from optical observations (see also the top panel of Figure 3). However, it can be unequivocally stated that the SDSS J0752 quasar has become active over the past 15 years and shows sporadic X-ray activity (e.g., MJD 54700–55400; Figure 3).

3 Results

3.1 Image of SDSS J0752

We detected an X-ray source (within the error radius 3.6″ with 90% confidence) at the location of SDSS J0752 indicated by optical observations $RA = 118.0735°$ and $Dec = 19.5952°$ (Zhang, 2022; see also https://skyserver.sdss.org/edr/en/sdss/skyserver/). At the same time, some of the coordinates of our X-ray source associated with SDSS J0752 were refined $RA = 118.0779°$ ($\alpha = 07^h52^m18^s.70$) and $Dec = +19.6351°$ ($\delta = +19°38'06''$, J2000.0) in accordance with the analysis of XTR/Swift data. The visual inspection of the source with the indicated coordinates showed the presence of an almost point-like source at the SDSS J0752 position and the absence of other nearby objects within a radius of 85″.

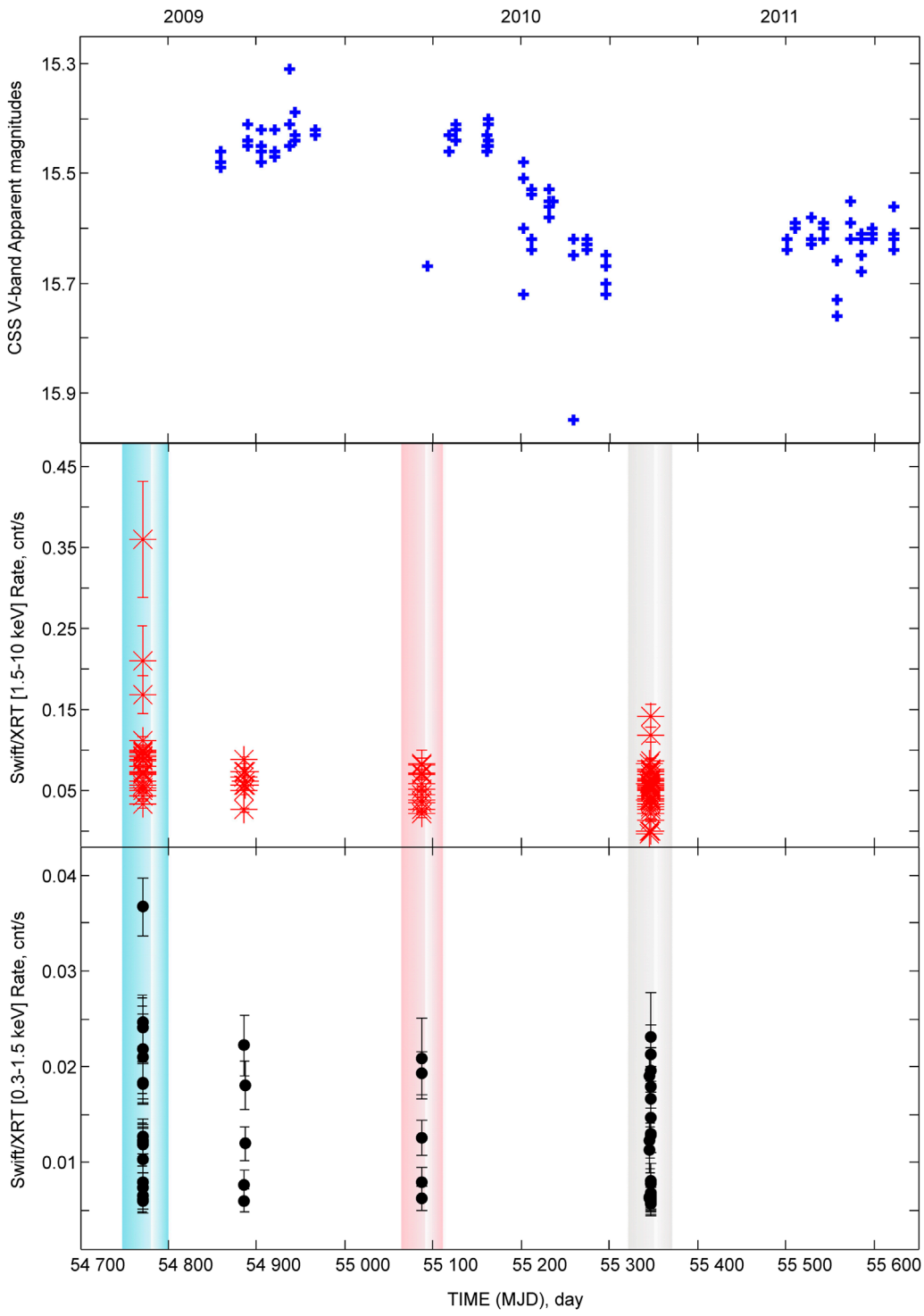

FIGURE 3
Evolution of the CSS V-band light curve (upper panel), the XRT/*Swift* [1.5–10 keV] count rate (middle panel), and the XRT/*Swift* [0.3–1.5 keV] count rate (bottom panel) of SDSS J0752 from 2008 to 2010. The phases LHS, IS, and HSS are marked with blue, gray, and red vertical strips, respectively, for which the corresponding spectra are presented in Figure 5.

3.2 X-ray light curve of SDSS J0752

We discovered the variability of SDSS J0752 in X-rays. The Swift/XRT light curves of this source in the 1.5–10-keV energy range (central panel) and in the 0.3–1.5-keV energy range (bottom panel) from 2008 to 2010 are presented in Figure 3. The figure shows light curves obtained with the binning mode by time. To test source variability within one observation, we set the time interval size

to ~100 s. The figure shows that the source is variable within one observation, even taking into account observational errors. Figure 3 also demonstrates the change in the maximum count rate achieved in each observation during the full source observation interval of 2008–2010. Comparing the source light curves in different energy bands showed that the main variability of SDSS J0752 is due to changes in the hard band (1.5–10 keV), although minor variability in the soft band (0.3–1.5 keV) also occurs. We also present CSS V-band light curve data, obtained from http://nesssi.cacr.caltech.edu/DataRelease/, to compare the variability of SDSS J0752 in different energy bands for the time interval MJD 54770 (October 2008) to 55650 (March 2011). The figure shows that the source is variable in both the X-ray and optical bands. Both bands show the tendency of the source to flare at MJD 54900–55100. In this case, the contribution of hard photons is significant for all states, but for MJD 55100, it is significantly smaller, which corresponds to a typical flare state for BHs (Titarchuk et al., 2023) and with a softened X-ray spectrum of the source (see the red spectrum in Figure 5). The phases LHS, IS, and HSS are marked with blue, gray, and red vertical strips, respectively, for which the corresponding spectra are presented in Figure 5 in the next section.

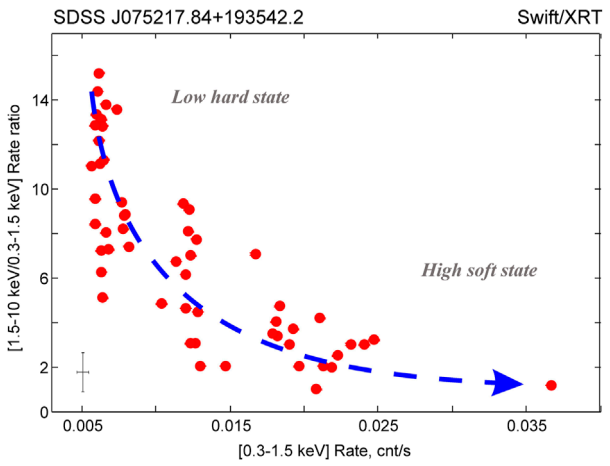

FIGURE 4
Hardness–intensity diagram (HID) for SDSS J0752 using the Swift/XRT observations (2008–2009) during spectral evolution from the high state to the low state. In the vertical axis, the hardness ratio (HR) is the ratio of the source count rates in the two energy bands: hard (1.5–10 keV) and soft (0.3–1.5 keV). The HR decreases with a soft source brightness in the 0.3–1.5-keV range (horizontal axis). For clarity, we plot only one point with error bars (in the bottom left corner) to demonstrate typical uncertainties for the count rate and HR. The blue dashed arrow indicates the direction of softening of radiation during the transition from the LHS to HSS.

3.3 Hardness–intensity diagram of SDSS J0752

By applying the Swift data of SDSS J0752, we defined the hardness ratio (HR) as a ratio of the hard and soft counts in the 1.5–10-keV and 0.3–1.5-keV bands, respectively. Figure 4 presents the hardness–intensity diagram (HID) for SDSS J0752 using the Swift/XRT observations (2008–2009) during the spectral evolution from the high state to the low state. The diagram demonstrates that different count-rate observations are related to different color regimes. The larger HR values correspond to harder spectra. For clarity, we plot only one point with error bars (in the bottom left corner) to demonstrate typical uncertainties for the soft count rate and HR. Figure 4 clearly shows that the HR monotonically decreases with the soft count rate (0.3–1.5 keV). This HID indicates the X-ray variability of SDSS J0752 with changing spectral states. This particular sample is similar to those of most flares of galactic X-ray binary transients (Homan et al., 2001; Belloni et al., 2006; Shaposhnikov and Titarchuk, 2009; Titarchuk and Seifina, 2009; Shrader et al., 2010; Munoz-Darias et al., 2014).

Below, we analyzed the SDSS J0752 spectrum in each observation to better understand the nature of this X-ray variability.

3.4 Spectral analysis of SDSS J0752

To fit the energy spectra of SDSS J0752, we used an XSPEC bulk motion Comptonization model (hereafter referred to as BMC model) [Titarchuk and Zannias (1998); Laurent and Titarchuk (1999)]. We also used a multiplicative `tbabs` model (Wilms et al., 2000), which takes into account the absorption by the neutral material. We assume that accretion onto a BH is described by two main zones [see Figure 1 in the study by Titarchuk and Seifina (2021)]: a geometrically thin accretion disk (e.g., the standard Shakura–Sunyaev disk; see SS73) and a transition layer (TL), which is an intermediate zone between the accretion disks, and a converging (bulk) region, which is assumed to exist below 3 Schwarzschild radii, $3R_S = 6GM_{\rm BH}/c^2$ [details given in the study by Titarchuk and Fiorito (2004)]. The spectral model parameters are the equivalent hydrogen absorption column density N_H; the photon index Γ; $\log(A)$, which is related to the Comptonized factor $f\,[=A/(1+A)]$; and the color temperature and normalization of the seed photon blackbody component kT_s and N_{bmc}, respectively. The parameter $\log(A)$ of the BMC component is fixed at two when the best-fit $\log(A) \gg 1$. In fact, for a sufficiently high $\log(A) \gg 1$ (and, therefore, a high value for A), the illumination factor f becomes a constant value close to 1 (i.e., the same as in the case of $\log(A) = 2$). We note that N_H was fixed at the galactic absorption level of 2.13×10^{22} cm^{-2} (Wilms et al., 2000).

Similar to the *bbody* XSPEC model, the normalization parameter of the BMC model is a ratio of the source (disk) luminosity L to the square of the distance d (see Eq. 1 in ST09):

$$N_{bmc} = \left(\frac{L}{10^{39}\text{erg/s}}\right)\left(\frac{10\ \text{kpc}}{d}\right)^2. \quad (1)$$

This encompasses an important property of our model. That is, using this model, one can accurately evaluate the normalization of the original "seed" component, which is presumably a correct $\dot{M}$ indicator (Seifina and Titarchuk, 2011). In turn,

$$L = \frac{GM_{BH}\dot{M}}{R_*} = \eta(r_*)\,\dot{m}L_{Edd}. \quad (2)$$

Here, $R* = r * R_S$ is an effective radius, where the main energy release takes place in the disk, $R_S = 2GM/c^2$ is the Schwarzschild radius, $\eta = 1/(2r*)$, $\dot{m} = \dot{M}/\dot{M}_{crit}$ is the dimensionless $\dot{M}$ in units

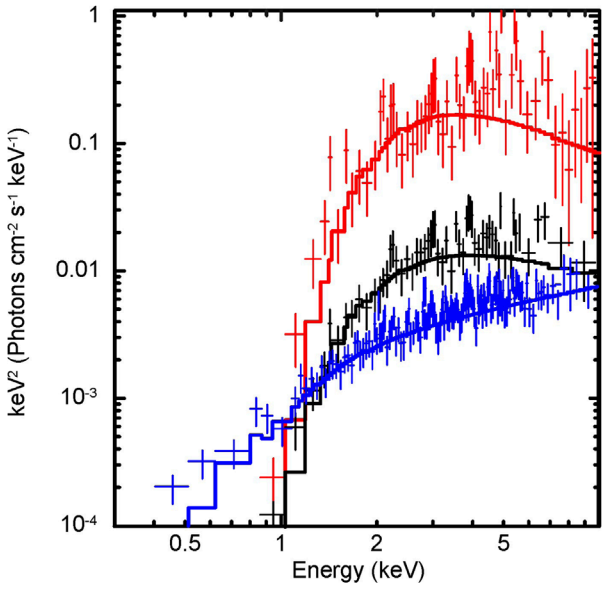

FIGURE 5
Three representative spectra of SDSS J0752 from *Swift* data with the best-fit modeling for the LHS (ID = 00038041001), IS (ID = 00039551001), and HSS (ID = 00038041002) in units of $E * F(E)$ using the `tbabs * bmc` model. The data are denoted by crosses, while the spectral model is shown by blue, black, and red histograms for each state.

of the critical mass accretion rate $\dot{M}_{crit} = L_{Edd}/c^2$, and L_{Edd} is the Eddington luminosity. The formulation of the Comptonization problem is given in the studies by Titarchuk et al. (1998); Titarchuk and Zannias (1998); Laurent and Titarchuk (1999); Borozdin et al. (1999); and Shaposhnikov and Titarchuk (2009).

Spectral analysis of the *Swift*/XRT data fits for SDSS J0752 provides a general picture of the source evolution. We can trace the change in the spectrum shape during the LHS–IS–HSS transition. Figure 5 shows three representative $E * F_E$ spectral diagrams for different states of SDSS J0752. Here, we put together spectra of the LHS, IS, and HSS to demonstrate the source spectral evolution from the low–hard to high–soft states based on the *Swift* observations. The data are presented as follows: the LHS (taken from observation 00038041001, blue), the IS (00039551001, black), and the HSS (00038041002, red) in units $E * F(E)$ fitted using the `tbabs * bmc` model. Exposure times are 3.6, 1.3, and 5.0 ks, respectively. It is worth noting that the source spectra were constructed based on the integral flux during the entire observation without taking into account binning to achieve a good signal-to-noise value. These spectra (blue, red, and black) are plotted for the LHS, IS, and HSS phases, marked with blue, gray, and red vertical stripes, respectively, as shown in Figure 3.

The best-fit parameters in the HSS (red spectrum in Figure 5) are $\Gamma = 2.9 \pm 0.6$, $kT_s = 130 \pm 5$ eV, $N = 8.2 \pm 0.6\ L_{34}/d^2_{10}$, and $\log(A) = -1.47 \pm 0.08$, for which the reduced chi-square value $\chi^2_{red} = 1.04$ for 964 degrees of freedom (dof); the best-fit model parameters for the IS (black spectrum) are $\Gamma = 2.2 \pm 0.6$, $kT_s = 140 \pm 3$ eV, $N = 2.3 \pm 0.8\ L_{33}/d^2_{10}$, and $\log(A) = -0.32 \pm 0.09$ ($\chi^2_{red} = 0.95$ for 288 dof); and, finally, the best-fit model parameters for the LHS (blue spectrum) are $\Gamma = 1.9 \pm 0.4$, $kT_s = 88 \pm 9$ eV, $N = 1.1 \pm 0.4\ L_{33}/d^2_{10}$, and $\log(A) = -3.58 \pm 0.07$ ($\chi^2_{red} = 1.06$ for 249 dof). A systematic uncertainty of 1% represents the instrumental flux calibration uncertainty and has been applied to all analyzed *Swift* spectra.

Analysis of the *Swift*/XRT data fits (Figure 6, pink circles) showed that Γ monotonically increases from 1.85 to 2.95 when the normalization of the spectral component (or $\dot{M}$) increases by a factor of approximately 15. We determined that the energy spectra of SDSS J0752 in all spectral states can be well modeled using a product of the `tbabs` and a `BMC` component.

We plotted the dependence of Γ on N_{bmc} (Figure 6) and discovered a linear section of a monotonic increase in the index with increasing N, which is proportional to the accretion rate $\dot{M}$. It is interesting that the dependence $\Gamma - N_{bmc}$ for high N_{bmc} clearly shows the area of index saturation at the level $\Gamma \sim 3$. This effect is well known as an index saturation (see ST09) (pink line in Figure 6). It was previously tested on a large number of sources with BHs of different masses [stellar-mass BHs; Titarchuk and Seifina (2009); Seifina and Titarchuk (2010); Titarchuk et al. (2014); Titarchuk and Seifina (2023)], intermediate-mass BHs (Titarchuk and Seifina (2016a); Titarchuk and Seifina (2016b)), and supermassive BHs (Titarchuk and Seifina (2017); Seifina et al. (2017); Seifina et al. (2018a); Seifina et al. (2018b); Titarchuk et al. (2020); Titarchuk et al. (2023)) and has established itself as a reliable indicator of the BH presence in the source (Titarchuk and Seifina (2009)). In addition to diagnosing the presence of a BH, this effect makes it possible to estimate the parameters of a BH object, such as mass and inclination.

3.5 A mass estimate of the SDSS J0752 secondary BH

We used a previously developed technique to estimate the BH mass, M_{SDSS} (Titarchuk et al., 2023). Previously, we did not know for which BH in the SDSS J0752 quasar the mass can be estimated using our X-ray data for SDSS J0752. We used the $\Gamma - N_{bmc}$ correlation to estimate a BH mass (see ST09 for details). This method ultimately (*i*) deals with a pair of BHs, for which Γ correlates with an increasing normalization N_{bmc} (which is proportional to the mass accretion rate $\dot{M}$ and a BH mass M; ST09, Eq. 7) and for which the saturation levels Γ_{sat} are the same, and (*ii*) calculates the scaling factor s_N, which allows us to determine the BH mass of the target object. It should also be emphasized that to estimate a BH mass using the following equation for the scale factor, the ratio of the distances to the *target* and *reference* sources is necessary:

$$s_N = \frac{N_r}{N_t} = \frac{m_r}{m_t}\frac{d_t^2}{d_r^2} f_G, \tag{3}$$

where N_r and N_t are the BMC normalizations of the spectra, $m_t = M_t/M_\odot$ and $m_r = M_r/M_\odot$ are the dimensionless BH masses with respect to solar mass, and d_t and d_r are distances to the *target* and *reference* sources, repectively. A geometrical factor, $f_G = \cos i_r/\cos i_t$, where i_r and i_r are the disk inclinations for the *reference* and *target* sources, respectively (see ST09, Eq. 7).

For appropriate scaling, we have to select X-ray sources (reference sources), which also show the effect of index saturation, and at the same Γ level as SDSS J0752 (target source). For reference

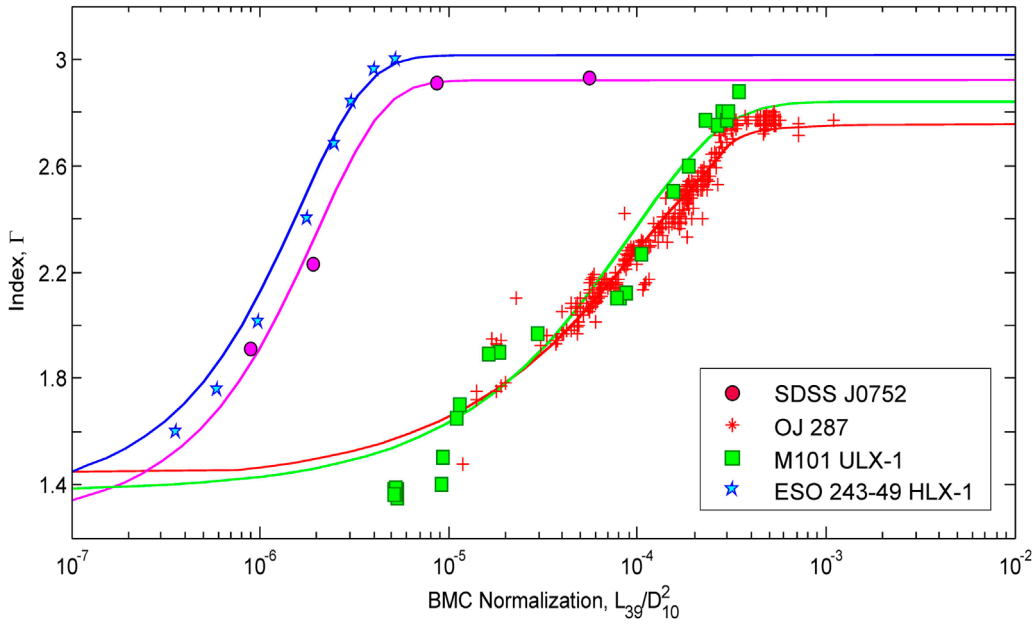

FIGURE 6
Scaling of the photon index Γ *versus* normalization N_{bmc} for SDSS J0752 (pink circles—target source) using the correlation for the reference sources OJ 287 (red crosses), ESO 243–49 HLX–1 (blue stars), and M101 ULX–1 (green squares).

sources, a BH mass, inclination, and distance must be well known. We found that OJ 287, M101 ULX–1, and HLX–1 ESO 243 can be used as the reference sources because these sources met all the aforementioned requirements to estimate a BH mass of the target source OJ 287 (see (i) and (ii) above).

Figure 6 shows how the photon index Γ evolves with normalization N (proportional to the mass accretion rate $\dot{M}$) in the blazar OJ 287 and in the SDSS J0752 quasar, where N is presented in units of L_{39}/d_{10}^2 (L_{39} is the source luminosity in units of 10^{39} erg/s and d_{10} is the distance to the source in units of 10 kpc).

In Figure 6, the correlations Γ *versus* N are self-similar for the *target* source (SDSS J0752), and two M101 ULX–1 and ESO 243–49 HLX–1 are ultra-luminous X-ray (ULX) sources. Moreover, these three sources have almost the same index saturation level Γ of approximately 2.8. We estimated a BH mass for SDSS J0752 using the scaling approach (see ST09). Figure 6 shows how the scaling method works shifting correlations relative to another. From these correlations, we could estimate N_t and N_r for SDSS J0752 and for the reference sources (Table 3). A value of $N_t = 5\times10^{-6}$ and N_r in units of L_{39}/d_{10}^2 are determined in the beginning of the Γ-saturation part [Figure 6; ST07; ST09; Titarchuk et al. (2014); Titarchuk and Seifina (2016a), Titarchuk and Seifina (2016b), Titarchuk and Seifina (2009)].

To determine the distance to SDSS J0752, we used the formula (for $z < 1$)

$$d_{SDSS} = z_{SDSS}c/H_0 \simeq 500\ Mpc, \tag{4}$$

where the redshift $z_{SDSS} = 0.117$ for SDSS J0752, $H_0 = 70.8 \pm 1.6$ $km^{-1}Mpc^{-1}$ is the Hubble constant, and $c = 3\times10^5$ km/s is the speed of light. This distance d_{SDSS} agrees with the luminosity distance estimate using Ned Wright's Javascript Cosmology Calculator[3] $d_{SDSS}^{NW} \sim 540$ Mpc (Wright, 2006).

A value of $f_G = \cos i_r/\cos i_t$ for the *target* and *reference* sources can be obtained using a trial inclination for SDSS J0752 $i_t = 50^o$ and for i_r (Table 3). As a result of the estimated target mass (SDSS J0752), m_t, we find that

$$m_t = f_G \frac{m_r}{s_N}\frac{d_t^2}{d_r^2}, \tag{5}$$

where $d_t = 500$ Mpc.

Applying Eq. 5, we can estimate m_t (Table 3), and we find that the secondary BH mass in SDSS J0752 is approximately $9\times(1\pm0.31)\times10^7$ $M_\odot$. To obtain this estimate with appropriate error bars, we need to consider error bars for m_r and d_r assuming, in the first approximation, errors for m_r and d_r only. We rewrote Eq. 5 as

$$m_t\left(1+\Delta m_t/m_t\right) = f_G\frac{m_r}{s_N}\frac{d_t^2}{d_r^2}\left(1+\Delta m_r/m_r\right)\left(1+2\Delta d_r/d_r\right). \tag{6}$$

Thus, we obtained errors for the m_t determination (see Table 3, second column for the *target* source) such that

$$\Delta m_t/m_t \sim \Delta m_r/m_r + 2\Delta d_r/d_r. \tag{7}$$

As a result, we find that $M_{SDSS} \sim 9\times10^7$ $M_\odot$ (M_{SDSS}= M_t) assuming that $d_{SDSS} = 500$ Mpc to SDSS J0752. Thus, we obtained a lower limit to the BH mass due to the unknown inclination. These results are given in Table 3.

3 https://www.astro.ucla.edu/wright/CosmoCalc.html

TABLE 3 Black hole (BH) masses and distances.

Reference Source	m_r, $M_\odot$	$i_r^{(a)}$, deg	N_r, L_{39}/d^2_{10}	$d_r^{(b)}$, Mpc
HLX–1				
ESO 243–49[(1)]	$(7.2\pm0.7)\times10^4$	75	4.2×10^{-6}	95 ± 10
M101 ULX–1[(2)]	$(3.7\pm0.6)\times10^4$	18	3×10^{-4}	6.9 ± 0.7
OJ 287[(3)]	$(1.25\pm0.5)\times10^8$	50	2.4×10^{-4}	1037 ± 10
Target source	m_t, $M_\odot$	$i_t^{(a)}$, deg	$d_t^{(b)}$, Mpc	
SDSS J0752	~9×(1±0.45)×10^7	50	500	That using ESO 243-49 as a reference source
SDSS J0752	~9×(1±0.45)×10^7	50	500	That using M101 ULX-1 as a reference source
SDSS J0752	Final estimate	50	500	As a standard deviation for a mean
	~9×(1±0.45)×10^7			$0.45/3^{1/2}=0.31$

(a) System inclination in the literature and (b) source distance found in the literature. (1) Titarchuk and Seifina (2016b); (2) Titarchuk and Seifina (2016a); and (3) Titarchuk et al. (2023).

In order to calculate the dispersion $\mathcal{D}$ of the arithmetic mean $\bar{m}_t$ for a BH mass estimate using different reference sources $\mathcal{D}$ (Table 3), it should be noted that

$$\mathcal{D}(\bar{m}_t) = D/n, \tag{8}$$

where D is the dispersion of m_r using each of the reference sources and $n=3$ is the number of the reference sources. As a result, we determined the mean deviation of the arithmetic mean,

$$\sigma(\bar{m}_t) = \sigma/\sqrt{n} \sim 0.31, \tag{9}$$

and finally, we obtained the following conclusion (Table 3):

$$\bar{m}_t \sim 9\times(1\pm0.31)\times10^7 \quad M_\odot. \tag{10}$$

It should be noted that in our calculations, we assume the angle between the normal to the secondary disk and the line of sight to be approximately 50°. However, the actual inclination may be different.

3.6 Secondary disk inclination estimate in SDSS J0752

The inclination of SDSS J0752 is still unknown. However, we can attempt to estimate it using the scaling method and the virial BH mass in SDSS J0752 from optical data (Zhang, 2022) under the assumption that the source of the X-ray variability is a secondary BH. Zhang (2022) reported that the virial mass of the secondary BH is approximately 8.8×10^7 $M_\odot$. Then, using the second scaling law (Titarchuk et al., 2023), we find the inclination of the secondary BH disk in SDSS J0752:

$$\cos(i_{SDSS}) = \cos(i_r)\,\frac{M_r}{M_t^{vir}}\left(\frac{d_r}{d_t}\right)^{-2}\frac{N_t}{N_r} \sim \cos(80°), \tag{11}$$

where we used ESO 243–49 HLX–1 as a *reference* source and parameters $M_r = 7.2\times10^4$ $M_\odot$, $M_t^{vir} = 8.8\times10^7$ $M_\odot$, $d_r = 95\pm10$ Mpc, $d_t = 500$ Mpc, $N_t = 5\times10^{-6}$, and $N_r = 4.2\times10^{-6}$.

As the inclination of the (mini)disk around the secondary BH based on its virial mass is estimated, we can refine our scaling estimate of a BH mass of the secondary BH. If we previously assumed $f_G = 1$, then clarifying the angle i_t leads to $f_G = 8$. Since the secondary disk should be observed almost edge-on, i.e., this angle i_t tends to be 90°, then the mass of the secondary BH component should be slightly larger, i.e., $\bar{m}_t \sim 7.2\times10^8$ $M_\odot$.

4 Discussion

We estimated the minidisk inclination of the secondary BH by combining scaling of the X-ray spectral properties of SDSS J0752 and the virial mass obtained from optical observations (CSS[4] and ASAS-SN[5] V-band light curve) of this quasar (Zhang, 2022). A high value of the inclination of the minidisk of the secondary BH was obtained ($\leq80^o$). However, it is necessary to emphasize that the IR and radio data available for SDSS J0752 are consistent with such a high minidisk inclination. It is known that SDSS J0752, a so-called blue quasar (Zhang, 2022), is a quasar whose IR is weakly absorbed. As a working hypothesis to explain the status of blue quasars, it was

4 http://nesssi.cacr.caltech.edu/DataRelease/

5 https://asas-sn.osu.edu/

argued that they are observed at a low inclination angle (Klindt et al., 2019) to the observer and are, thus, weakly subject to IR absorption. According to this hypothesis, blue quasars are fundamentally different from the so-called red quasars, whose radiation is predominantly red at optical wavelengths due to the presence of dust in the line of sight. However, Klindt et al. (2019) ruled out orientation as the cause of the differences between red and blue quasars based on an analysis of quasar radio properties using FIRST data (1.4 GHz/6 μm).

However, even in the case of the "face-on" orientation of the main disk of the SDSS J0752 quasar, when we observe the galaxy disk almost from the pole, the high inclination of the secondary BH (mini)disk we obtained is consistent with the fact that the orbit of the secondary BH is oriented perpendicular to the plane of the main disk around the primary BH. This is consistent with our orbital flare scenario (Figure 1), in which the orbit of the secondary BH does not coincide with the galactic plane but makes a significant angle, in our case, ~80°. Therefore, we clearly observe periodic X-ray and optical flares during the orbital passage of a secondary BH through the disk around the primary BH (i.e., through the disk of the galaxy).

We obtained a fairly low temperature of the seed photons kT_s from the inner part of the disk around the secondary BH (80–115 eV). This is consistent with calculations of the X-ray spectrum arising from the innermost part of the source, based on first-principle physical models, taking into account the Comptonization of soft disk photons by hot electrons of the Compton cloud originating from the innermost part of the disk and from the converging flow of the BH. Indeed, in the case of a $10^8 M_\odot$ BH, the peak temperature of the disk is relatively low, $kT_s < 1$ keV$/(M_{BH}/10M_\odot)^{1/4}$, i.e., approximately 20–100 eV, and its thermal peak is in the UV energy range.

We proceed with a scenario of orbital rotation of a binary system in the center of the SDSS J0752 quasar, consisting of two BHs of higher and lower mass (Figure 1), which explains its X-ray variability. In this case, a heavier BH is surrounded by a powerful accretion disk, and a lighter BH, surrounded by the minidisk, rotates around the primary BH in a plane different from the equatorial plane of the accretion disk of the primary BH, crossing it twice during the orbital period (6.4 years). We also assumed that when a secondary BH passes through the disk around the primary BH, "tidal disruption" of nearby parts of the disk occurs. As a result, a partial destruction and subsequent replenishment of matter from the accretion minidisk around the secondary BH takes place [see a similar process given in the study by Chan et al. (2021)]. In this case, a powerful transition minidisk is developed around the secondary BH with the subsequent accretion of material from the transition minidisk onto the secondary BH. This provides an increase in luminosity in the X-ray/optical/radio bands.

To complete our analysis, we list other possible reasons leading to the variability in quasar emission. It should be also taken into account that this variability of quasars may be associated with changes in the emission of their jets. This source is a weak radio emitter and is not classified as "radio loud." By the conventional definition of radio loudness, it is $R = L_{radio}/L_{bolometric} \sim 10$. For this object, it is $R \sim 0.3$. A recent structural analysis of 447 of the radio sources in the northern sky at 15 GHz (Lister et al., 2021) showed variations in the position angle of the jets with an average amplitude of 10°–50° on a timescale of approximately 10 years. For some sources, variations reach 200°. There are several scenarios that could explain this behavior, for example, orbital motion in a binary BH (Begelman et al., 1980). The Lense–Thirring effect (Lense and Thirring, 1918; Thirring, 1918) in a binary system with a rotating BH is widely discussed. In this case, fluctuations in the internal orientation of the jet are caused by the precession of the accretion disk, the rotation axis of which is shifted relative to the rotation axis of the BH (Caproni et al., 2004). For example, based on observations made over 22 years in 170 epochs, a study of the structure of the jet in the radio Galaxy M87 showed a periodic change in the position angle of the jet with a peak-to-peak amplitude of ~10° and a period of T ~11 years on scales ~600–2,500 r_g (Cui et al., 2023). The periodicity of the light curve in the optical range and variations in the position angle of the jet in the quasar 3C 120 suggest the existence of a precession of the jet caused by the Lense–Thirring effect with a period of 12.3 years (Caproni and Abraham, 2004). The same is also shown for the jet in M81*, the precession period of which is estimated at ~7 years (von Fellenberg et al., 2023). A detailed analysis of the orientation oscillations of other jets also indicates their periodicity and possible connection with precession, for example, PKS 2131–021 (O'Neill et al., 2022) ($T \sim$ 22 years), PG 1553 + 113 (Lico et al., 2020), 4C 38.41 (Algaba et al., 2019) ($T = 23 \pm 5$ years), 3C 279 (Abraham and Carrara, 1998) ($T \sim$ 22 years), 3C 273 (Abraham and Romero, 1999) ($T \sim$ 16 years), and OJ 287 (Britzen et al., 2018) ($T \sim$ 12 years). This list may be supplemented by SDSS J0752, but this requires additional research.

One can argue that the emission from this quasar object comes from a jet. However, we do not see any serious arguments for this statement. A particularly important point regards the fitting of *Swift* X-ray spectra. One could think that our spectral models contain too many components and, thus, they could not be fitted to low-resolution *Swift* data since there would then be many more free parameters than actual independent data bins. This is not the case because our continuum spectral model is an XSPEC model consisting of the BMC component. The spectral model parameters are the equivalent hydrogen absorption column density N_H; the photon index Γ; $\log(A)$, which is related to the Comptonized factor f; and the color temperature and normalization of the seed photon blackbody components kT_s and N, respectively.

Since the more massive BH is not active in the X-rays, then the active culprit for the X-ray flares, for example, in M87, is precisely the secondary (less massive) BH. It is this activity that underlies the X-ray scaling and timing analysis methods, and their results relate to the smaller BH of this binary system in M87. Now, it is not surprising that a BH mass, according to X-ray estimates by Titarchuk et al. (2020), turned out to be two orders of magnitude less than results of the EHT method (Akiyama et al., 2019) and the classical gas and stellar dynamic approach (Gebhardt et al., 2011; Walsh et al., 2013).

5 Conclusion

The optical periodic variability of the SDSS J0752 quasar has raised several questions regarding whether the source contains one or two BHs. It was very important to identify the X-ray characteristics indicating the duality of this quasar. In this paper, we demonstrated that an X-ray source coupled to an optical source exhibits flux variability in the 0.3–10 keV energy range by a factor of 15. At the same time, the X-ray spectra of SDSS J0752 undergo transitions from the LHS to the IS and then to the HSS (Figure 5) based on data obtained using the XRT on board the *Swift* observatory. We fitted the SDSS J0752 energy spectrum to a Comptonization model and described the evolution of the spectrum parameters. The temperature of the seed disk photons turned out to be very low (kT_s = 0.08–0.15 keV), the degree of disk illumination varied in a wide range (illumination factor f = 0.1–1), and the disk luminosity in the soft X-ray range $L_{0.3-10keV}$ showed a monotonic increase during the state evolution—the LHS → IS → HSS—with a factor of 10 and was correlated with the optical flash of SDSS J0752 ($N_{bmc} = (0.1-8) \times L_{34}/d_{10}^2$). In addition, we discovered the saturation of the photon index with the mass accretion rate in SDSS J0752, which allowed us to scale the secondary BH in this object using the scaling method. We thus determined a mass of 9×10^7 $M_\odot$ for the secondary BH. We showed that a scenario in which two supermassive BHs at the center of the SDSS J0752 quasar form an orbital pair, and the less massive secondary BH periodically crosses/pierces the disk around the more massive primary BH, can be applied to SDSS J0752. Thus, we associated an increase in the X-ray flux in SDSS J0752 with intersections of the disk of the primary BH with the secondary BH. In addition, we estimated the orbital inclination of the secondary BH, i = 80°, based on a combination of our scaling approach and virial BH mass estimates obtained by Zhang (2022).

Data availability statement

The original contributions presented in the study are included in the article/Supplementary Material; further inquiries can be directed to the corresponding author.

Author contributions

LT: writing–review and editing and writing–original draft. ES: writing–review and editing, writing–original draft, supervision, methodology, and investigation.

Funding

The author(s) declare that no financial support was received for the research, authorship, and/or publication of this article.

Acknowledgments

The authors thank the anonymous reviewer for the careful reading of the manuscript and for providing valuable comments. The authors thank Chris Shrader for the careful reading and editing of the manuscript. We acknowledge the UK *Swift* Science Data Centre at the University of Leicester for the supplied data. This paper used the data from the CSS projects http://nesssi.cacr.caltech.edu/DataRelease/.

Conflict of interest

The authors declare that the research was conducted in the absence of any commercial or financial relationships that could be construed as a potential conflict of interest.

Publisher's note

References

Abraham, Z., and Carrara, E. A. (1998). The precessing jet in 3C 279. *Astrophys. J.* 496, 172–176. doi:10.1086/305387

Abraham, Z., and Romero, G. E. (1999). Beaming and precession in the inner jet of 3C 273. *Astron. Astrophys* 344, 61–67.

Akiyama, K., Alberdi, A., Alef, W., Asada, K., Azulay, R., Baczko, A., et al. (2019). First M87 event horizon telescope results. VI. The shadow and mass of the central black hole. *Astrophys. J. Lett.* 875, L6. doi:10.3847/2041-8213/ab1141

Algaba, J. C., Rani, B., Lee, S. S., Kino, M., Park, J., and Kim, J.-Y. (2019). Exploring the morphology and origins of the 4C 38.41 jet. *Astrophys. J.* 886, 85. doi:10.3847/1538-4357/ab4b45

Begelman, M. C., Blandford, R. D., and Rees, M. J. (1980). Massive black hole binaries in active galactic nuclei. *Nature* 287, 307–309. doi:10.1038/287307a0

Belloni, T., Parolin, I., Del Santo, M., Homan, J., Casella, P., Fender, R. P., et al. (2006). INTEGRAL/RXTE high-energy observation of a state transition of GX 339–4. *Mon. Not. R. Astron. Soc.* 367, 1113–1120. doi:10.1111/j.1365-2966.2006.09999.x

Boroson, T. A., and Lauer, T. R. (2009). A candidate sub-parsec supermassive binary black hole system. *Nature* 458, 53–55. doi:10.1038/nature07779

Borozdin, K., Revnivtsev, M., Trudolyubov, S., Shrader, Ch., and Titarchuk, L. (1999). Do the spectra of soft X-ray transients reveal bulk-motion inflow phenomenon? *it Astrophys. J.* 517, 367–380. doi:10.1086/307186

Britzen, S., Fendt, C., Witzel, G., Qian, S.-J., Pashchenko, I. N., Kurtanidze, O., et al. (2018). OJ 287: deciphering the Rosetta stone of blazars. *Mon. Not. R. Astron. Soc.* 478, 3199–3219. doi:10.1093/mnras/sty1026

Caproni, A., and Abraham, Z. (2004). Can long-term periodic variability and jet helicity in 3C 120 be explained by jet precession? *Mon. Not. R. Astron. Soc.* 349, 1218–1226. doi:10.1111/j.1365-2966.2004.07550.x

Caproni, A., Mosquera Cuesta, H. J., and Abraham, Z. (2004). Observational evidence of spin-induced precession in active galactic nuclei. *Astrophys. J.* 616, L99–L102. doi:10.1086/426863

Chan, C.-H., Piran, T., and Krolik, J. H. (2021). High-energy emission from tidal disruption events in active galactic nuclei. *Astrophys. J.* 914, 107. doi:10.3847/1538-4357/abf0a7

Chen, Y.-C., Liu, X., Liao, W.-T., Holgado, A. M., Guo, H., Gruendl, R., et al. (2020). Candidate periodically variable quasars from the dark energy Survey

and the sloan digital sky Survey. *Mon. Not. R. Astron. Soc.* 499, 2245–2264. doi:10.1093/mnras/staa2957

Cui, Y., Hada, K., Kawashima, T., Kino, M., Lin, W., Mizuno, Y., et al. (2023). Precessing jet nozzle connecting to a spinning black hole in M87. *Nature* 621, 711–715. doi:10.1038/s41586-023-06479-6

Drake, A. J., Djorgovski, S. G., Mahabal, A., Beshore, E., Larson, S., Graham, M. J., et al. (2009). First results from the Catalina real-time transient Survey. *Astrophys. J.* 696, 870–884. doi:10.1088/0004-637X/696/1/870

Eracleous, M., Boroson, T. A., Halpern, J. P., and Liu, J. (2012). A large systematic search for close supermassive binary and rapidly recoiling black holes. *Astrophys. J. Suppl. Ser.* 201, 23. doi:10.1088/0067-0049/201/2/23

Evans, P. A., Beardmore, A. P., Page, K. L., Osborne, J. P., O'Brien, P. T., Willingale, R., et al. (2009). Methods and results of an automatic analysis of a complete sample of Swift-XRT observations of GRBs. *Mon. Not. R. Astron. Soc.* 397, 1177–1201. doi:10.1111/j.1365-2966.2009.14913.x

Evans, P. A., Beardmore, A. P., Page, K. L., Tyler, L. G., Osborne, J. P., Goad, M. R., et al. (2007). An online repository of Swift/XRT light curves of γ-ray bursts. *Astron. Astrophys.* 469, 379–385. doi:10.1051/0004-6361:20077530

Gebhardt, K., Adams, J., Richstone, D., Lauer, T. R., Faber, S. M., Gultekin, K., et al. (2011). The black hole mass in M87 from gemini/NIFS adaptive optics observations. *Astrophys. J.* 729, 119. doi:10.1088/0004-637x/729/2/119

Homan, J., Wijnands, R., van der Klis, M., Belloni, T., van Paradijs, J., Klein-Wolt, M., et al. (2001). Correlated X-ray spectral and timing behavior of the black hole candidate xte j1550–564: a new interpretation of black hole states. *ApJS* 132, 377–402. doi:10.1086/318954

Klindt, L., Alexander, D. M., Rosario, D. J., Lusso, E., and Fotopoulou, S. (2019). Fundamental differences in the radio properties of red and blue quasars: evolution strongly favoured over orientation. *Mon. Not. R. Astron. Soc.* 488, 3109–3128. doi:10.1093/mnras/stz1771

Kochanek, C. S., Shappee, B. J., Stanek, K. Z., Holoien, T. W.-S., Thompson, T. A., Prieto, J. L., et al. (2017). The all-sky automated Survey for Supernovae (ASAS-SN) light curve server v1.0. *Publ. Astron. Soc. Pac.* 129, 104502. doi:10.1088/1538-3873/aa80d9

Kollatschny, W., Weilbacher, P. M., Ochmann, M. W., Chelouche, D., Monreal-Ibero, A., Bacon, R., et al. (2020). NGC 6240: a triple nucleus system in the advanced or final state of merging. *Astron. Astrophys.* 633, A79. doi:10.1051/0004-6361/201936540

Komberg, B. V. (1967). A binary system as a quasar model. *Astron. Zh.* 44, 906–907.

Koss, M., Mushotzky, R., Treister, E., Veilleux, S., Vasudevan, R., Miller, N., et al. (2011). Chandra discovery of a binary active galactic nucleus in Mrk 739. *Astrophys. J. Lett.* 735, L42. doi:10.1088/2041-8205/735/2/L42

Koss, M. J., Treister, E., Kakkad, D., Casey-Clyde, J. A., Kawamuro, T., Williams, J., et al. (2023). UGC 4211: a confirmed dual active galactic nucleus in the local universe at 230 pc nuclear separation. *Astrophys. J. Lett.* 942, L24. doi:10.3847/2041-8213/aca8f0

Laurent, P., and Titarchuk, L. (1999). The converging inflow spectrum is an intrinsic signature for a black hole: Monte Carlo simulations of comptonization on free-falling electrons. *Astrophys. J.* 511, 289–297. doi:10.1086/306683

Laurent, P., and Titarchuk, L. (2011). Spectral index as a function of mass accretion rate in black hole sources: Monte Carlo simulations and an analytical description. *Astrophys. J.* 727, 34. doi:10.1088/0004-637X/727/1/34

Lense, J., and Thirring, H. (1918). On the influence of the proper rotation of central bodies on the motions of planets and moons according to einstein's theory of gravitation. *Phys. Z.* 19, 156–163.

Lico, R., Liu, J., Giroletti, M., Orienti, M., Gomez, J. L., Piner, B. G. al., et al. (2020). A parsec-scale wobbling jet in the high-synchrotron peaked blazar PG 1553+113. *Astron. Astrophys.* 634, id.A87. doi:10.1051/0004-6361/201936564

Lister, M. L., Homan, D. C., Kellermann, K. I., Kovalev, Y. Y., Pushkarev, A. B., Ros, E., et al. (2021). Monitoring of jets in active galactic nuclei with VLBA experiments. XVIII. Kinematics and inner jet evolution of bright radio-loud active galaxies. *Astrophys. J.* 923, 30. doi:10.3847/1538-4357/ac230f

Liu, T., Gezari, S., Burgett, W., Chambers, K., Draper, P., Hodapp, K., et al. (2016). A systematic search for periodically varying quasars in pan-STARRS1: an extended baseline test in medium deep Survey field MD09. *Astrophys. J.* 833, 6. doi:10.3847/0004-637X/833/1/6

Molnar, S. M., Schive, H.-Y., Birkinshaw, M., Chiueh, M. T., Musoke, G., and Young, A. J. (2017). Hydrodynamical simulations of colliding jets: modeling 3C 75. *Astrophys. J.* 835, 57. doi:10.3847/1538-4357/835/1/57

Munoz-Darias, T., Fender, R. P., Motta, S. E., and Belloni, T. M. (2014). Black hole-like hysteresis and accretion states in neutron star low-mass X-ray binaries. *Mon. Not. R. Astron. Soc.* 443, 3270–3283. doi:10.1093/mnras/stu1334

O'Neill, S., Kiehlmann, S., Readhead, A. C. S., Aller, M. F., Blandford, R. D., Liodakis, I., et al. (2022). The unanticipated phenomenology of the blazar PKS 2131-021: a unique supermassive black hole binary candidate. *Astrophys. J. Lett.* 926, L35. doi:10.3847/2041-8213/ac504b

Paris, I., Petitjean, P., Aubourg, E., Myers, A. D., Streblyanska, A., Lyke, B. W., et al. (2018). The sloan digital sky Survey quasar catalog: fourteenth data release. *Astron. Astrophys.* 613, 51. doi:10.1051/0004-6361/201732445

Seifina, E. (2024). "Active galaxy nuclei: current state of the problem," in *Astron. Astrophys. Transact* (Cambridge: Cambridge Scientific Publishers) 34 (2). Arxiv:2311.14830[astro-ph.GA].

Seifina, E., Chekhtman, A., and Titarchuk, L. (2018b). NGC 4051: black hole mass and photon index-mass accretion rate correlation. *Astron. Astrophys.* 613, 48. doi:10.1051/0004-6361/201732235

Seifina, E., and Titarchuk, L. (2010). On the nature of the compact object in SS 433: observational evidence of X-ray photon index saturation. *Astrophys. J.* 722, 586–604. doi:10.1088/0004-637X/722/1/586

Seifina, E., and Titarchuk, L. (2011). On the constancy of the photon index of X-ray spectra of 4U 1728-34 through all spectral states. *Astrophys. J.* 738, 128. doi:10.1088/0004-637X/738/2/128

Seifina, E., Titarchuk, L., and Ugolkova, L. (2018a). Scaling of X-ray spectral properties of a black hole in the Seyfert 1 galaxy NGC 7469. *Astron. Astrophys.* 619, 21. doi:10.1051/0004-6361/201833169

Seifina, E., Titarchuk, L., and Virgilli, E. (2017). Swift J164449.3+573451 and Swift J2058.4+0516: black hole mass estimates for tidal disruption event sources. *Astron. Astrophys.* 607, 38. doi:10.1051/0004-6361/201730869

Shakura, N. I., and Sunyaev, R. A. (1973). Black holes in binary systems. Observational appearance. *Astron. Astrophys.* 24, 337–355.

Shaposhnikov, N., and Titarchuk, L. (2007). Determination of black hole mass in Cygnus X-1 by scaling of spectral index-QPO frequency correlation. *Astrophys. J.* 663, 445–449. doi:10.1086/518110

Shaposhnikov, N., and Titarchuk, L. (2009). Determination of black hole masses in galactic black hole binaries using scaling of spectral and variability characteristics. *Astrophys. J.* 699, 453–468. doi:10.1088/0004-637X/699/1/453

Shappee, B. J., Prieto, J. L., Grupe, D., Kochanek, C. S., Stanek, K. Z., De Rosa, G., et al. (2014). The man behind the curtain: X-rays drive the UV through NIR variability in the 2013 active galactic nucleus outburst in NGC 2617. *Astrophys. J.* 788, 48. doi:10.1088/0004-637X/788/1/48

Shrader, C. R., Titarchuk, L., and Shaposhnikov, N. (2010). New evidence for a black hole in the compact binary Cygnus X–3. *Astrophys. J.* 718, 488–493. doi:10.1088/0004-637X/718/1/488

Thirring, H. (1918). Uber die Wirkung rotierender ferner Massen in der Einsteinschen Gravitationstheorie. *Phys. Z.* 19, 33–39.

Titarchuk, L., and Seifina, E. (2009). Discovery of photon index saturation in the black hole binary GRS 1915+105. *Astrophys. J.* 706, 1463–1483. doi:10.1088/0004-637X/706/2/1463

Titarchuk, L., and Seifina, E. (2016a). Scaling of the photon index vs mass accretion rate correlation and estimate of black hole mass in M101 ULX–1. *Astron. Astrophys.* 585, A94. doi:10.1051/0004-6361/201526122

Titarchuk, L., and Seifina, E. (2016b). ESO 243–49 HLX–1: scaling of X-ray spectral properties and black hole mass determination. *Astron. Astrophys.* 595, A101. doi:10.1051/0004-6361/201527840

Titarchuk, L., and Seifina, E. (2017). BL Lacertae: X-ray spectral evolution and a black-hole mass estimate. *Astron. Astrophys.* 602, 113. doi:10.1051/0004-6361/201630280

Titarchuk, L., and Seifina, E. (2021). Detection of a high-temperature blackbody hump in black hole spectra - the strongly redshifted annihilation line. *Mon. Not. R. Astron. Soc.* 501, 5659–5678. doi:10.1093/mnras/staa3961

Titarchuk, L., and Seifina, E. (2023). MAXI J1348–630: estimating the black hole mass and binary inclination using a scaling technique. *Astron. Astrophys.* 669, 57. doi:10.1051/0004-6361/202244585

Titarchuk, L., Seifina, E., Chekhtman, A., and Ocampo, I. (2020). Spectral index–mass accretion rate correlation and evaluation of black hole masses in AGNs 3C 454.3 and M 87. *Astron. Astrophys.* 633, A73. doi:10.1051/0004-6361/201935576

Titarchuk, L., Seifina, E., and Shaposhnikov, N. (2014). Black hole mass determination in the X-ray binary 4U 1630–47: scaling of spectral and variability characteristics. *Astrophys. J.* 789, 57. doi:10.1088/0004-637X/789/1/57

Titarchuk, L., Seifina, E., and Shrader, Ch. (2023). OJ 287: a new BH mass estimate of the secondary. *Astron. Astrophys.* 671, A159. doi:10.1051/0004-6361/202345923

Titarchuk, L., Shaposhnikov, N., Seifina, E., Ruffini, R., and Vereshchagin, G. (2010). Discovery of photon index saturation in the black hole binaries. *AIP Conf. Proc.* 1205, 168–176. doi:10.1063/1.3382325

Titarchuk, L., and Zannias, T. (1998). The extended power law as an intrinsic signature for a black hole. *Astrophys. J.* 493, 863–872. doi:10.1086/305157

Titarchuk, L. G., and Fiorito, R. (2004). Spectral index and quasi-periodic oscillation frequency correlation in black hole sources: observational evidence of two phases and phase transition in black holes. *Astrophys. J.* 612, 988–999. doi:10.1086/422573

Titarchuk, L. G., Mastichiadis, A., and Kylafis, N. D. (1998). Mechanisms for high-frequency quasi-periodic oscillations in neutron star and black hole binaries. *Astrophys. J.* 499, 315–328. doi:10.1086/305642

Voggel, K. T., Seth, A. C., Baumgardt, H., Husemann, B., Neumayer, N., Hilker, M. L., et al. (2022). First direct dynamical detection of a dual supermassive black hole system at sub-kiloparsec separation. *Astron. Astrophys.* 658, A152. doi:10.1051/0004-6361/202140827

von Fellenberg, S. D., Janssen, M., Davelaar, J., Zajacek, M., Britzen, S., Falcke, H., et al. (2023). Radio jet precession in M 81 $*$. *Astron. Astrophys.* 672, L5. doi:10.1051/0004-6361/202245506

Walker, R. C., Hardee, P. E., Davies, F. B., Ly, C., and Junor, W. (2018). The structure and dynamics of the subparsec jet in M87 based on 50 VLBA observations over 17 Years at 43 GHz. *Astrophys. J.* 855, 128. doi:10.3847/1538-4357/aaafcc

Walsh, J. L., Barth, A. J., Ho, L. C., and Sarzi, M. (2013). The M87 black hole mass from gas-dynamical models of space telescope imaging spectrograph observations. *Astrophys. J.* 770, 86. doi:10.1088/0004-637X/770/2/86

Wilms, J., Allen, A., and McCray, R. (2000). On the absorption of X-rays in the interstellar medium. *Astrophys. J.* 542, 914–924. doi:10.1086/317016

Wright, E. L. (2006). A Cosmology calculator for the world wide web. *Publ. Astron. Soc. Pac.* 118, 1711–1715. doi:10.1086/510102

Zhang, X.-G. (2022). A 6.4-yr optical quasi-periodic oscillations in SDSS J075217.84+193542.2: a new candidate for central binary black hole system. *Mon. Not. R. Astron. Soc.* 512, 1003–1011. doi:10.1093/mnras/stac540